CHEMICAL PHYSICS

Laser-based temperature control to study the roles of entropy and enthalpy in polymer-nanopore interactions

Christopher E. Angevine[1], Joseph W.F. Robertson[2]*, Amala Dass[3], Joseph E. Reiner[1]*

Single-molecule approaches for probing the free energy of confinement for polymers in a nanopore environment are critical for the development of nanopore biosensors. We developed a laser-based nanopore heating approach to monitor the free energy profiles of such a single-molecule sensor. Using this approach, we measure the free energy profiles of two distinct polymers, polyethylene glycol and water-soluble peptides, as they interact with the nanopore sensor. Polyethylene glycol demonstrates a retention mechanism dominated by entropy with little sign of interaction with the pore, while peptides show an enthalpic mechanism, which can be attributed to physisorption to the nanopore (e.g., hydrogen bonding). To manipulate the energetics, we introduced thiolate-capped gold clusters [$Au_{25}(SG)_{18}$] into the pore, which increases the charge and leads to additional electrostatic interactions that help dissect the contribution that enthalpy and entropy make in this modified environment. These observations provide a benchmark for optimization of single-molecule nanopore sensors.

INTRODUCTION

The study of polymer energetics in nanoporous systems began in earnest in the 1970s with investigations of partition coefficients of macromolecules into zeolites and gels among other nanoporous materials (*1*). This spawned theoretical investigations into the static and dynamic properties of confined polymer chains (*2*, *3*). This work focused on applying scaling laws toward understanding intrapore diffusion coefficients and polymer partitioning coefficients, both of which could be studied with techniques that used bulk porous materials to measure the ensemble properties of the molecules. While these ensemble methods provided critical insight into polymer-pore interactions, the advent of single-molecule nanopore sensing (*4*–*6*) provides a platform for the study of polymer-pore dynamics on a more fundamental level.

Nanopore-based resistive pulse sensing is an effective tool for single-molecule analysis (*7*, *8*). This sensing provides label-free and high-throughput (~10 events/s to 100 events/s) detection, as well as the ability to modify the local environment (such as the force via voltage and temperature in some cases). Effective resistive-pulse sensing requires that molecules spend a measurable amount of time within the pore so that the corresponding current blockades are easily measurable. Given the typical pore dimensions (≈5 nm), a molecule that experiences no interactions with the pore should escape in less than 1 μs. Thus, for molecules to be observed in the pore with a low-pass cutoff frequency of 10 kHz, there must be a free energy barrier against escape that can be parameterized by enthalpic and entropic components (*9*). Characterizing this free energy barrier offers insight into the mechanism for retention of polymer analytes in nanopore sensors and molecular mechanisms of membrane transport proteins (*10*), which can improve precision, understanding, and optimization of nanopore sensing systems. Moreover, this characterization can more broadly elucidate about the mechanisms dictating solute transport through transmembrane channels (*11*).

Using the Fokker-Plank equations (*12*–*14*) and detailed analysis of polymer theory (*15*, *16*), connections can be made between polymer-pore dynamics and the free energy barrier for a polymer to escape the nanopore (*6*). Subsequently, a large number of reports have studied polymer nanopore interactions providing both detailed coarse-grained models for the potential well (*15*, *17*–*19*) and chemically specific analytical models (*20*). The most comprehensive models for the free energy of a polymer confined in a nanopore included potential energies from excluded volume effect, vibrational modes of the intermolecular bonds, external electric fields and electrostatic interactions (*19*). Further extensions have included the interactions of the polymer with solvent and electrolyte components as well (*20*), which provides the ability to model voltage-dependent effects for neutral polymers in nanopores.

While most work discusses entropy as the dominant contributor to the free energy barrier (*9*, *21*, *22*), there is evidence that enthalpy can play a critical role, particularly in modified systems that enhance the electrostatic interactions available within the pore (*23*, *24*). One successful approach to separating the thermodynamic components used the replacement of weakly interacting cations, such as K^+, with a noninteracting cation (i.e., Li^+) (*25*). However, a more direct method would be to measure polymer-nanopore kinetics as a function of temperature to construct Arrhenius plots from which the enthalpy and entropy can be unambiguously extracted. Although temperature control of a nanopore apparatus is available through infrared lamps, or sealed Peltier devices, the cumbersome and slow nature of these experiments (i.e., temperature changes over minute time scales) has limited the number of detailed thermal studies to just a few examples (*26*–*31*).

To overcome the challenges of static, external temperature-control methods, we used a laser-based heating approach (*31*) that allows dynamic control of the local temperature. Optical heating can be achieved through direct excitation of the vibrational modes in water with infrared light (*31*, *32*) or indirectly through nanoplasmonic-assisted heating (*33*, *34*) and excitation of electronic modes in semiconductor materials (*35*). This work will focus on

[1]Department of Physics, Virginia Commonwealth University, Richmond, VA 23284, USA. [2]Biophysics Group, Microsystems and Nanotechnology Division, National Institute of Standards and Technology, Gaithersburg, MD 20899, USA. [3]Department of Chemistry and Biochemistry, University of Mississippi, University, MS 38677, USA. *Corresponding author. Email: jereiner@vcu.edu (J.E.R.); joey.robertson@nist.gov (J.W.F.R.)

direct infrared heating that has been used to demonstrate thermal control of DNA unzipping for nanopore analysis (*31*, *35*). Using dynamic control, data for nearly continuous Arrhenius plots can be collected in short times (≈10 s). We demonstrate this technique by directly measuring the enthalpy and entropy components of the free energy for polymer escape for small peptides and polyethylene glycol (PEG) from the α-hemolysin (αHL) pore and the $Au_{25}(SG)_{18}$-modified αHL complex. The analysis here uses a self-consistent picture of the energetic landscape by connecting the free energy difference between the polymer in the pore and the polymer in the bulk (i.e., partition coefficient) to the free energies of polymer capture and escape. This connection yields a relationship between the polymer residence time kinetics and the free energy of escape from the pore, which provides a more complete picture of the interactions that are critical for the optimization of a nanopore sensor.

RESULTS

Theoretical background

Here, we model the polymer-pore interaction with a free energy profile along an unspecified reaction coordinate. Figure 1 shows a schematic illustration of this free energy profile in and around the nanopore. This energy profile contains three distinct levels: a bulk solution level, a pore occupied level, and a transition level between these two states that serves to limit entry and exit of polymer analyte into and away from the pore. Our goal is to extract the enthalpy and entropy components of the transition barrier using a laser-based heating methodology. To better understand the relative magnitude of these three levels, we begin with room temperature estimates of the free energy difference between the bulk and pore occupied states (ΔG^0_{total}). This can be found from the polymer partition coefficient

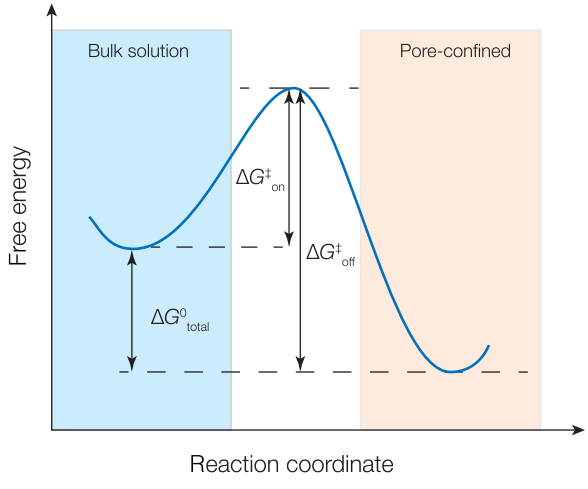

Fig. 1. Proposed free energy scheme for polymer capture and release from a nanopore. Analyte from outside the pore overcomes a barrier $\Delta G^{\ddagger}_{on}$ to enter the pore. Analyte resides inside the pore in a lower energy state relative to the bulk. Escape from the pore back into the bulk solution requires overcoming the free energy barrier to escape $\Delta G^{\ddagger}_{off}$. This study focuses on laser-based extraction of the entropy and enthalpy components of $\Delta G^{\ddagger}_{off}$. See the main text for a discussion on estimates of $\Delta G^{\ddagger}_{on}$ and ΔG^{0}_{total}.

$$\Pi = \frac{1}{N_A V_{pore} C_{bulk}} \frac{\tau_{in}}{\tau_{total}} = \exp\left(\frac{\Delta G^0_{total}}{k_B T}\right) \quad (1)$$

where N_A is Avogadro's number, V_{pore} is the pore volume, C_{bulk} is the polymer concentration in the bulk solution, τ_{in} is the total occupation time of analyte in the pore, τ_{total} is the total measurement time, k_B is Boltzmann's constant, and T is the absolute temperature. This definition of the partition coefficient normalizes out the pore volume, which means that Π is a measure of the lifetime of a polymer in the pore compared to a polymer in a pore-sized volume in bulk solution. This convention leads to a partition coefficient greater than 1 and thus a free energy of polymer occupation in the pore greater than the bulk, as used previously by others (*36*, *37*). In addition, we note that all analysis throughout is performed at a single applied potential (70 mV) and each free energy value is to be interpreted as corresponding to that applied potential (i.e., $\Delta G^0_{total} = \Delta G^0_{total}$ at 70 mV).

The free energy barrier to be captured by the pore ($\Delta G^{\ddagger}_{on}$) can be estimated from the on-rate capture of polymer into the pore k_{on} using the seminal Berg-Purcell relation (*38*)

$$k_{on} = 4DaC_{bulk} \exp\left(-\frac{\Delta G^{\ddagger}_{on}}{k_B T}\right) \quad (2)$$

Here, D is the diffusion coefficient of the analyte and a is the pore radius. For the purposes of this analysis, we neglect any modification of the diffusion coefficient for polymers near the pore entrance where the applied field will cause drift-dominated flow. A more complete description of the on-rate kinetic process and connection to the free energy of capture can be found elsewhere (*39*).

To estimate the relative magnitude of the different energy barriers used herein, we performed nanopore measurements on polydisperse PEG, monodisperse PEG with 28 repeat units (PEG_{28}), and the three peptides angiotensin 1 (AT1), angiotensin 2 (AT2), and neurotensin (NT) under various solution conditions at room temperature. A complete description of experimental conditions along with a summary of results for the free energy barriers can be found in the Supplemental Materials. These values are in reasonable agreement with previous measurements (*25*) and, as we outline below, provide a means to extract the entropic and enthalpic components of the free energy barrier to escape from the pore.

Residence time blockade distributions are well described by single exponential functions that allow us to treat the polymer-nanopore system as a chemical interaction with a simplified transition-state reaction scheme (*20*, *40*). Thus, the mean blockade residence time and the free energy barrier to analyte escape $\Delta G^{\ddagger}_{off}$ are related by the following expression

$$\tau = \tau_0(T) \exp\left(\frac{\Delta G^{\ddagger}_{off}}{k_B T}\right) \quad (3)$$

Here, τ_0 is the attempt time to escape from the pore, which will depend on the solution temperature (*20*). The enthalpic, $\Delta H^{\ddagger}_{off}$, and entropic, $\Delta S^{\ddagger}_{off}$, components of the free energy barrier to escape can be found from the slope and intercept of the natural log of the mean residence time versus the inverse temperature as follows

$$\ln\left(\frac{\tau}{\tau_0}\right) = \frac{\Delta G^{\ddagger}_{off}}{k_B}\left(\frac{1}{T}\right) = \frac{\Delta H^{\ddagger}_{off}}{k_B}\left(\frac{1}{T}\right) - \frac{\Delta S^{\ddagger}_{off}}{k_B} \quad (4)$$

Thus, the mean residence time, normalized by the attempt time measured at various temperatures, can be used to estimate the entropy and enthalpy of the free energy barrier for polymer escape from the pore. Calculating the attempt time can be difficult and model dependent (*41*), which limits the effectiveness of Eq. 3 to extract $\Delta H^{\ddagger}_{off}$ and $\Delta S^{\ddagger}_{off}$. To address this, we note that the predetermined values for ΔG^{0}_{total} and $\Delta G^{\ddagger}_{on}$ from Eqs. 1 and 2 and the fact that $\Delta G^{\ddagger}_{off} = \Delta G^{0}_{total} + \Delta G^{\ddagger}_{on}$ (see Fig. 1) can be used to fix values for the estimated attempt time at room temperature. In brief, the attempt time becomes an adjustable parameter so that the entropy and enthalpy components extracted from Eq. 4 are in agreement with the $\Delta G^{\ddagger}_{off}$ value found from Eqs. 1 and 2 (i.e., $\Delta G^{\ddagger}_{off} = \Delta H^{\ddagger}_{off} - T\Delta S^{\ddagger}_{off}$). A more complete description of the attempt time estimates and the temperature dependence of the attempt time used throughout this manuscript are provided in the Supplemental Materials.

Experimental background

Constructing Arrhenius plots described in Eq. 4 requires the ability to heat the solution temperature in and around the nanopore. Here, we use a laser-based heating mechanism, which offers several improvements over bulk heating methods. Rapid control of local temperatures with infrared light can avoid some of the instabilities in protein and membrane systems often encountered in single-molecule nanopore devices. Figure 2A illustrates the principle of operation. A 1444-nm laser was intensity-modulated with a sinusoidal waveform at 0.25 Hz by an acousto-optic modulator (AOM) and directed to the back aperture of a microscope objective (4×, numerical aperture 0.2) that focused the light onto a lipid bilayer membrane containing a single αHL pore. At this wavelength, water absorbs infrared light ($\alpha \approx 30\ cm^{-1}$), which provides heating within the laser focal spot ($V_{focal} \approx 10$ pl). To investigate intra-pore thermodynamics, two well-characterized polymer systems—PEG and peptides (AT1, AT2, and NT)—and negatively charged glutathione-capped gold nanoclusters [$Au_{25}(SG)_{18}$] were investigated. Both molecules and clusters interact with the nanopore, reversibly allowing for the ionic current to be monitored for extended periods of time. $Au_{25}(SG)_{18}$ reduces the conductance by approximately 25% with mean residence times on the order of tens of seconds (Fig. 2B). The presence of these clusters in the pore leads to a 20-fold increase of the polymer residence time in the pore and thus improves the prospects of nanopore sensing near-neutral polymers (*8*). However, the mechanism for this cluster-induced enhancement remains unclear and partially motivates the free energy studies here.

To extract the enthalpic and entropic free energy components, ionic current is recorded at room temperature to produce a baseline data point in the Arrhenius plot; we then modulate the laser intensity resulting in open pore current between approximately 200 and 350 pA. The open pore current can then be used to estimate the temperature using a second-order polynomial that converts the open pore current to temperature (*27*, *31*, *33*) (more details can be found in the Supplemental Materials). This corresponds to a temperature range of approximately 25° to 50°C (*27*, *31*, *33*). We can assign a residence time, blockade depth, and solution temperature to each blockade event. This conversion is highlighted in Fig. 2 (C and D) for both PEG_{28} and AT1 under open channel conditions. A similar calibration scheme is used when $Au_{25}(SG)_{18}$ clusters are confined in the pore (Supplementary Materials). The defining characteristics of the polymer-induced blockades are the magnitude of the current interruption (i.e., blockade depth) and the residence time. The peptides and PEG samples analyzed here produce well-resolved featureless blockades from which the blockade depth can be used to estimate the polymer size (*42*). Here, the residence time was used to examine the role of thermodynamic properties of the molecules in detecting and characterizing the polymers. To justify using simplified models for the characterization of a polymer, we first measured the residence time distribution of PEG_{28} and AT1 at two temperatures (Fig. 2, E and F, respectively). In every case, the blockade distribution is well described by a single exponential decay that allows us to treat the polymer-nanopore interaction as a chemical interaction with a simplified transition-state reaction scheme (i.e., Eq. 3) (*20*, *40*).

To create Arrhenius plots, resistive pulses were recorded for approximately 5 min during a temperature sinusoidal modulation (period = 0.25 Hz). The residence time τ was then calculated for temperatures binned with approximately 0.4 K precision (see Supplementary Materials for details). The resulting data were then plotted and analyzed to extract the enthalpy and entropy of the free energy barrier to polymer escape. Figure 3 illustrates the advantages of the laser-driven temperature control (dynamic control); AT1 was observed with laser-based heating and compared to a similar experiment using static-Peltier control temperature control. The purpose of this comparison was to ensure that the dynamic laser-based temperature modulation does not produce any unexpected systematic biases. The agreement between the laser-based heating and the bulk solution heating suggests that the laser heater does not introduce spurious artifacts (i.e., through convective flow or radiative transfer) into the system. We note that because the data collection (including temperature equilibration between points) required more than 30 min to generate a dataset that contained three discrete data points, replicate measurements for bulk temperature manipulation are typically prohibitive.

Ionic strength dependence for homopolymer PEG: Open pore

Clearly, the dynamic heating methodology presented herein provides another, more sensitive, tool to probe polymer-pore interactions. As a first demonstration of dynamic analysis, we focus on the free energy components of PEG confinement in an αHL pore as a function of the solvent ionic strength. The αHL pore is the workhorse of the biological nanopore sensing community. It has been well characterized and consists of a trans-side lumen and cis-side vestibule separated by a constriction ring with diameter ≈1.5 nm (*43*). Previous estimates of the trans-side lumen volume, where polymers will reside throughout our measurements, range from 10 to 50 nm^3 (*44*). Here, we model the pore lumen as a right circular cylinder with an average pore diameter of 2.2 nm and a length of 5.5 nm, yielding an overall pore volume (trans-side lumen) of 21 nm^3. Previous work has shown that PEG residence times in the αHL pore depend strongly on the ionic strength and nature of the electrolyte (*25*, *45*–*47*). Given the connection between increasing the residence time and the efficacy of a nanopore sensor, understanding the mechanism connecting ionic strength and residence time represents an ideal example of the use of dynamic heating to better understand the nanopore as a sensor.

Potassium chloride has been thoroughly studied and shown to weakly interact with PEG (*20*). In nanopore spectroscopy, this association leads to an increase of PEG residence time in the nanopore with the effect increasing with cation concentration (*20*, *40*). The molecular mechanism for the increased retention time is unclear. Speculation on the mechanism has suggested increased interaction strength between the polymer and the pore (*47*, *48*), decreased solubility of the polymer as the solvent stops behaving as a good

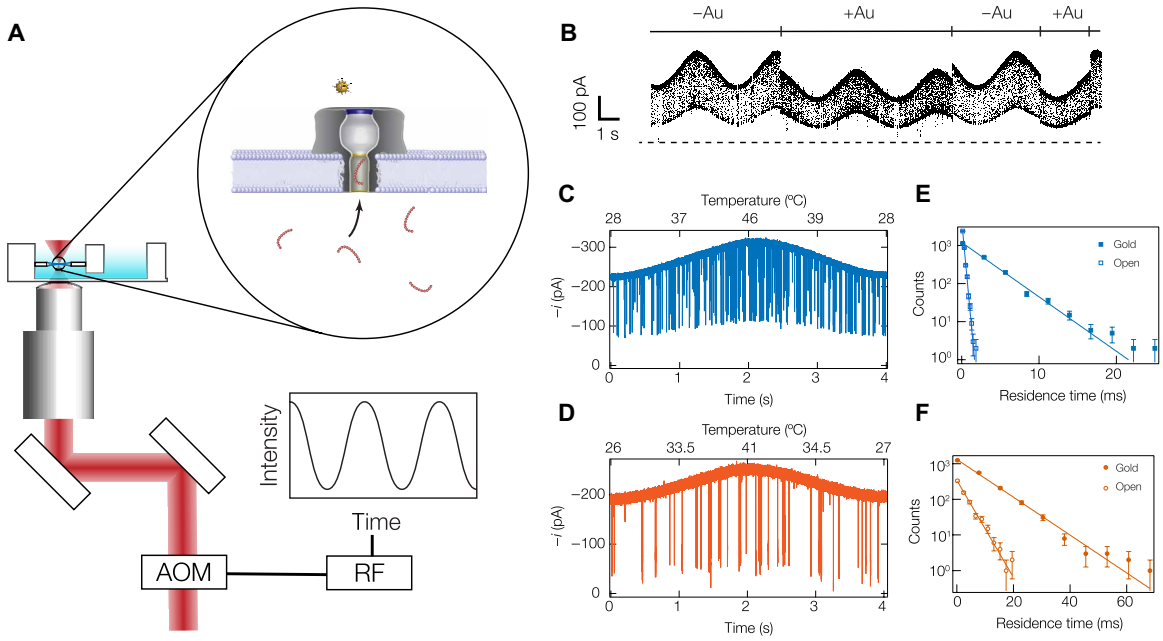

Fig. 2. Illustration of the experimental setup and corresponding heating traces. (**A**) Schematic representation of the experimental setup. (**B**) Typical current trace for PEG_{28} interacting with the nanopore as Au-cluster partition, into and out of the vestibule of αHL. (**C**) and (**D**) show the temperature-calibrated current for PEG_{28} and AT1, respectively, as the polymers interact with the open pore. The current (and temperature) is modulated by the infrared laser through one period of oscillation. (**E**) PEG-αHL residence time distributions are shown at 24°C with a Au-cluster (filled square) and open pore (open square) configuration. (**F**) AT1-αHL residence time distributions are shown at 24°C with a Au-cluster (filled square) and open pore (open square) configuration. Data shown were collected in 3 M KCl under 70 mV applied transmembrane potential. Ground voltage is referenced to the trans-side of the pore throughout all experiments. Error bars in (E) and (F) are estimated from 1 SD calculated as the square root of the counts.

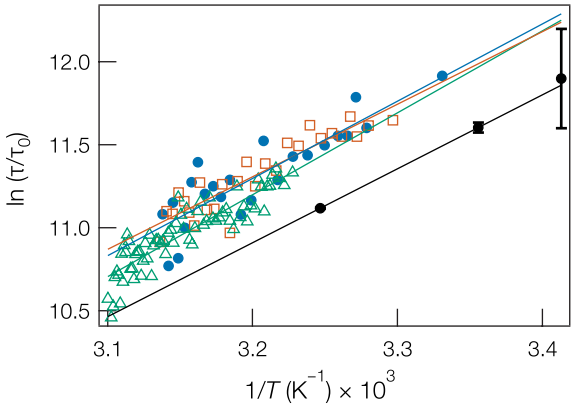

Fig. 3. Comparison of Arrhenius plots for bulk heating and laser-based heating. Arrhenius plots produced by the laser-based dynamic (open symbols, three different pores) and Peltier-based bulk (filled black circles, one pore) heating protocols show consistency between the methods. The solid lines are least squares linear fits to each dataset. The static heating conditions correspond to temperature control via a PID-controlled Peltier device embedded in the analysis chamber. The dynamic heating conditions correspond to temperature control via a 1444-nm laser modulated with an AOM. The static experiments produced three discrete temperatures. The error bars for the static datasets were estimated from the standard deviation of observed residence times. Representative data are from AT1 at 70 mV in 3 M KCl (pH 7.2).

solvent (*25*), or changes in the entropic barrier to transport (*49*–*52*). The temperature-dependent studies here shed light on the mechanism. We note that the limited range of ionic strengths reported here (3.0 < [KCl] < 3.8 M) results from the fact that KCl crashes out of solution at higher ionic strength (KCl maximum solubility ≈ 4 M in the presence of PEG) and PEG residence times at elevated temperatures fall well below the inverse detection bandwidth of our system (B^{-1} = 100 μs) for [KCl] < 3.0. Nevertheless, compelling results can be seen over our reported concentration range.

It is well established that the residence time for PEG increases with ionic strength (*20*, *25*, *45*, *46*, *53*). This phenomenon is primarily due to the interaction of cations with the polymer molecule and confirmed here in Fig. 4A, which shows that the PEG_{28} residence time of both the open pore (blue) and cluster-occupied pore (orange) grows with increasing ionic strength. This behavior can be understood from the overall free energy of escape as a function of ionic strength in Fig. 4B, which has been attributed to a microscopic description in which PEG forms a complex with K^+ to PEG-K^+_n that imparts polyelectrolyte-type properties on the polymer (*20*, *40*). Under this scenario, we can model the escape barrier into entropic contributions related to tension along the molecule as it exits the pore through the region where the local electric field is largest (*54*). This alters the enthalpic barrier by reducing the mean coordination number of the ions bound to the polymer. When the escape barrier is separated into enthalpic (Fig. 4C) and entropic (Fig. 4D) contributions, it is apparent that ionic strength alters the contribution of both enthalpy and entropy for both the open pore (blue) and the gold cluster occupied

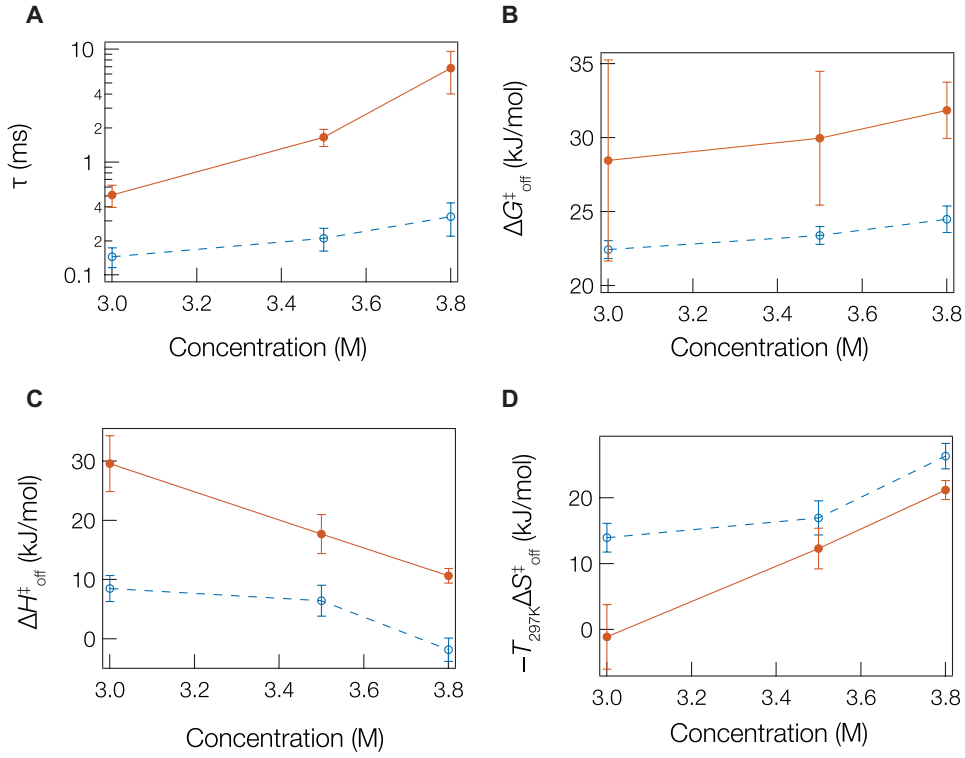

Fig. 4. Mean residence time and free energy contributions (enthalpy and entropy) of the escape barrier for the open pore (blue) and cluster-occupied pore (orange) for PEG_{28} as a function of KCl salt concentration. (**A**) The mean residence time increases with increasing ionic strength and the mean residence time increases by about an order of magnitude with a cluster present in the pore. (**B**) $\Delta G^{\ddagger}_{off}$ shows similar trends to the residence time behavior, validating the thermodynamic description of the PEG-pore kinetics. (**C**) $\Delta H^{\ddagger}_{off}$ increases with the gold in the pore and partially explains the gold cluster behavior. (**D**) $\Delta S^{\ddagger}_{off}$ (scaled as $-T\Delta S^{\ddagger}_{off}$, $T = 297$ K) increases with ionic strength, which explains the residence time dependence and shows that the entropic component dominates the open pore behavior. In addition, the gold cluster in the pore reduces the entropic component, and this can be understood by the fact that the cluster modifies the confined volume within the pore. See the main text for details. All data were taken in KCl electrolyte buffered to pH 7.2 with tris under a 70-mV applied transmembrane potential. Each data point corresponds to weighted averages over three different pores, and the error bars correspond to ±1 standard error (SE). The solid and dashed lines are guides to the eye only.

pore (orange) as well. While the residence time increases for the PEG with cation concentration, the enthalpic component of the PEG-pore interaction decreases (Fig. 4C). This is counterintuitive if the dominant interaction is a van der Waals interaction between the pore and the polymer. However, we note that the entropic component of the escape barrier increases with ionic strength (Fig. 4D) (here, the entropy component is scaled as $-T\Delta S^{\ddagger}_{off}$ to facilitate comparison with the enthalpic component). We can attribute reduced significance of $\Delta H^{\ddagger}_{off}$ to charge screening by the electrolyte and $-T\Delta S^{\ddagger}_{off}$ to increased stiffness of the polymer as it binds more cations in the transition region between the bulk and pore. This combination leads to an increasing residence time with increasing ionic strength provided that the rate of change for the entropy exceeds that of the enthalpy, which it does in this case. Given the positive correlation between PEG residence time and ionic strength (*25*, *40*, *45*, *53*), it appears that the entropic component of the free energy barrier is the critical factor in determining PEG-pore interactions as ionic strength is increased in a pore that has little to no excess charge.

To check the validity of these reported values for $\Delta H^{\ddagger}_{off}$ and $-T\Delta S^{\ddagger}_{off}$, we use simplified models for the energetic components confining the polymer to the pore. Beginning with the enthalpy component, we note that the PEG is confined to the trans lumen region of the pore under an applied transmembrane field. Previous numerical studies have shown that in the ionic strength conditions reported here, PEG_{28} weakly binds about 2e of charge (*40*). Under an applied 70-mV transmembrane field, the charge will be confined only partway across this potential drop [i.e., the PEG only experiences ca. 30% of the field drop in the trans lumen region of the pore (*54*)]. From this, we can estimate $\Delta H^{\ddagger}_{off} = 0.3qV_{app} = 4.2$ kJ/mol, which is in reasonable agreement with the values reported in Fig. 4C. In addition, the entropic component of the polymer transition barrier can be estimated from the free energy required to completely stretch a polymer chain $T\Delta S^{\ddagger}_{off} = r^2 k_B T/(nb^2)$, where r is the average end-to-end distance of the polymer, n is the polymer repeat number, and b is the size of each monomer subunit (*55*). For PEG_{28}, we have the following parameters: $r = 2.1$ nm, $n = 28$, and $b = 0.1464$ nm (*56*, *57*), which yield $-T\Delta S^{\ddagger}_{off} = 6.8\ k_B T = 16.8$ kJ/mol at room temperature. As with the enthalpic change, this too is in reasonable agreement with the reported values in Fig. 4D. These results verify our kinetic approach to estimating the enthalpy and entropy components of the free energy barrier to polymer escape.

Ionic strength dependence for homopolymer PEG: Cluster-occupied pore

In addition to the open pore analysis, we performed thermodynamic analysis for the gold cluster–occupied pore and found that enthalpy

is increased nearly fourfold with respect to the open pore case and the entropy is reduced in the presence of the gold. We believe that these two observations can be understood by the fact that clusters add two additional barriers to transport: an increased entropic barrier at the constriction point of the αHL β barrel (*43*) and an enthalpic change due to Coulombic interaction between the cation-bound PEG and the negatively charged gold clusters. It appears that the Coulombic attraction dominates even under extremely high ionic strength conditions. This may be explained by the fact that increasing ionic strength increases the number of cations bound to the PEG and thus the attraction between the PEG and gold cluster. Regardless of the exact mechanism, Fig. 4 highlights two important conclusions. The first is that for the open pore, the entropic component of the free energy barrier to escape for PEG appears to dominate the kinetics and suggests that to increase the PEG residence time, one should focus on the polymer degrees of freedom both inside the pore and in the transition region between the pore and bulk solution. The second conclusion is that although entropy drives the PEG-pore interaction, it is possible to modify the enthalpy (via charge) to increase the PEG-pore interaction time, which is a route to superior size selectivity by the pore (*30*, *58*).

Polydisperse PEG

The results in Fig. 4 focus on one particular PEG size ($n = 28$). However, a benefit from the single-molecule analysis is the ability to isolate data from precise polymer sizes. With individual n-mers of PEG resolved, the relative energetic contributions can be expressly estimated for each monomer-length increase in the polymer (Fig. 5). To achieve sufficient resolution, ionic current was recorded with static laser power until a sufficient number of molecules were observed to characterize the residence time for n-mers ranging from $n = 18$ to $n = 40$. The data were processed and binned in a two-dimensional histogram (Fig. 5A). A more thorough discussion on the construction of the histogram in Fig. 5A can be found in the Supplementary Materials.

To extract the thermodynamic information, the residence time was measured at seven static temperatures with laser heating (Fig. 5B) and the thermodynamic information was calculated from these values. Previous work suggests that PEG is excluded from the pore by the entropic-spring effect that becomes dominant at ≈3000 g/mol or $n \approx 68$ (*46*), which corresponds to an estimate of the largest PEG molecule that completely fits in the β barrel ≈3400 g/mol ($n \approx 77$) (*30*). We stress that the data presented here are well below this pore-filling regime, yet it shows a appreciable shift in the energetics of the polymer-pore system.

As shown previously (*20*), $\Delta G^{\ddagger}_{off}$ for the polymer capture smoothly increases with increasing polymer size. However, a closer inspection shows that $\Delta H^{\ddagger}_{off}$ decreases with polymer size in a nonlinear fashion while the entropic term, $-T\Delta S^{\ddagger}_{off}$ (at 297 K), increases at an approximately 50% higher rate (Fig. 5C). These data show a subtle transition in the behavior of the polymer from an enthalpic-dominated process for small molecules to an entropic-dominated process as the polymer exceeds $n = 25$. In this regime, the diameter of the polymer is approximately equal to the diameter of the β barrel at its widest point and 1.3 times the diameter at the narrowest constriction in the pore (*43*) as estimated by the hydrodynamic radius of PEG in bulk solution under good solvent conditions [$2R_h = 2.0$ nm for $n = 27$ (*57*, *59*)].

The increase in $-T\Delta S^{\ddagger}_{off}$ with polymer size is attributed to the difference between entropy in the pore and entropy as the polymer leaves the pore. Thus, the polymer degrees of freedom increase more rapidly with increasing polymer size inside the pore than through the transition state, which is consistent with a model where the polymer is stretched in the electric field through the escape transition. Conversely, $\Delta H^{\ddagger}_{off}$ decreases with increasing polymer size, which seems counterintuitive. One would expect larger polymers to chelate more cations and thus increase the enthalpic barrier to escape. However, this is not the case and could be attributed to a combination of charge repulsion between bound cations on the PEG chain and other effects related to the transition out of the pore that may impede the ability for larger polymers to chelate additional cations in the transition state.

Overall, the ability to separate the entropic and enthalpic components of the free energy barrier to PEG escape highlights the fact that the mechanism that causes the increasing residence time with increasing PEG mass is dominated by the entropic component of the free energy barrier, which was also observed for the case of homopolymer PEG in different ionic strength solutions. The laser-based heating approach provides a sensitive tool to explore these free energy components and better understand the mechanisms that drive polymer-pore interactions.

Peptides

PEG interactions with the αHL pore provide an excellent test case from which to fine-tune and optimize free energy analysis. Figures 4 and 5 highlight the effectiveness of the laser-based heating methodology and elucidate the mechanisms that give rise to the PEG interactions with both the open and cluster-occupied pore. These results are consistent with previous efforts (*25*), and this motivates studies of more exotic polymers besides PEG. Nanopore resistive pulse sensors have emerged as a viable sensor for peptides and proteins (*60*, *61*). Careful choice of both the chemistry and geometry of the pore has enabled size-selective (*62*–*64*), shape-selective (*65*, *66*), and even sequence-specific detection of proteins and peptides (*67*, *68*). Here, we will focus on the interaction of peptides with the αHL pore. Temperature studies help to expand our understanding of the free energy profile, which, in turn, could help optimize the conditions required for accurate peptide sensing and identification.

To better understand the interaction of peptides with the open and cluster-occupied pore, we performed laser-based thermodynamic analysis on three commercially available peptides: AT2, AT1, and NT. These polypeptides fall within the mass range of the PEG molecules that were analyzed and each has high-quality NMR structures: NT (2OYV) (*69*), AT1 (1N9U), and AT2 (1N9V) (*70*). These structures are reproduced in fig. S6 in two different forms to highlight the differences between them. Cursory investigation reveals that AT2 is a relatively stiff peptide. The side-chain rotations reveal four conformations containing one hydrogen bond and one conformation with two hydrogen bonds among the 20 resolved structures. AT1 retains the primary structure of AT2 with two additional residues (histidine and leucine) on the C terminus of the peptide. From these data, 16 hydrogen bonds were observed in the 20 resolved structures with no more than 3 appearing in any structure. In addition to the increased number of hydrogen bonds, the AT1 has stable secondary structures with these bonds appearing to span multiple residues, rather than simply adjacent residues. This should have marked effects on the ability of the AT1 peptides to freely explore

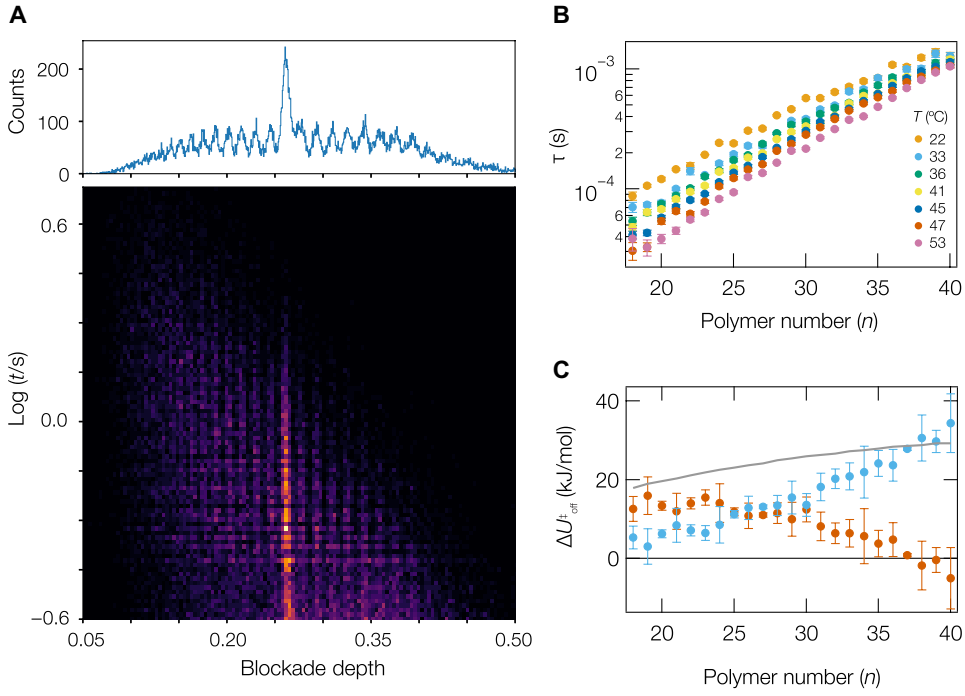

Fig. 5. The free energy profile of polydisperse PEG in the open pore configuration reveals size-dependent shifts in the free energy components. (**A**) Two-dimensional histogram of a PEG mixture provides a range of discrete polymer data. (**B**) Residence time of the extracted data as a function of temperature. (**C**) Relative contributions of $\Delta H^{\ddagger}_{off}$ (red) and $-T\Delta S^{\ddagger}_{off}$ (cyan) to the Gibbs free energy at 297 K. All data were collected in 3.5 M KCl with an applied potential of 70 mV. The solid gray line shows the overall free energy of escape calculated from the entropy and enthalpy components. This shows that the entropic component of the free energy dominates the enthalpic component as PEG size increases. The polydisperse PEG mixture consists of PEG2000:PEG1000:PEG_{28} at 10 μM:10 μM:2 μM concentrations. The error bars in (C) correspond to ±1 SD calculated from $n = 3$ different pores.

their structural space, particularly when confined within the nanopore. The NT structures contain no resolved hydrogen bonds, and the structure is best characterized by two structurally conserved regions separated by a flexible hinge (*69*). Prior work using αHL to analyze these peptides showed that despite the nearly 10-fold longer pore residence time compared to similarly sized PEG, the blockade depth for peptides was well predicted by modified volume exclusion effects (*42*). The gold cluster–occupied pore did not lead to as large an increase in the peptide residence time as compared to PEG (Fig. 2, E and F). Thermodynamic studies can shed light on these observations.

Figure 6A shows the mean residence time and Fig. 6B shows the overall free energy of escape of these three peptides for the open (blue) and cluster-occupied (orange) pores. The residence time increases with increasing mass in a manner similar to PEG (Figs. 4A and 5B), while the free energy shows little change across the three peptides (within corresponding error bars). To better understand this, we measured $\Delta H^{\ddagger}_{off}$ (Fig. 6C) and $-T_{297K}\Delta S^{\ddagger}_{off}$ (Fig. 6D) for the escape barrier of the peptides with and without a cluster in the pore. For each of the peptides, the gold cluster results inw only a two- to threefold increase in the residence time, suggesting that the peptides cannot interact efficiently across the constriction at the end of the hemolysin β barrel (*43*). This may result from the longer persistence length of amino acid chains than PEG (*57*, *71*, *72*). A direct comparison of the free energy components and residence times for PEG and peptides can be found in fig. S5 in the Supplementary Materials.

The open pore peptide data shed some light on the nature of the peptide-pore interactions. For each of the peptides, the $\Delta H^{\ddagger}_{off}$ strongly favors remaining in the pore, while $\Delta S^{\ddagger}_{off}$ favors exclusion (i.e., $\Delta H^{\ddagger}_{off} > 0$, $-T_{297K}\Delta S^{\ddagger}_{off} < 0$). This enthalpic dominated polymer-pore interaction most likely results from hydrogen bonding with one or two residues within the pore. We rule out electrostatic interactions because the enthalpy component of all three peptides is nearly identical despite the fact that the overall net charge on AT2 and AT1 is considerably less than NT (*42*). In any event, this contrasts with PEG that showed that the increasing residence time with increasing ionic strength (Fig. 4) and mass (Fig. 5) was primarily due to the entropic component of the free energy barrier to escape.

Comparing entropic and enthalpic barriers for escape between the three peptides in the gold-free pore highlights the slight differences between them. For instance, while the $\Delta H^{\ddagger}_{off}$ is essentially the same for both angiotensin peptides, there is a slight increase in enthalpy between AT1 and NT. In addition, $-T_{297K}\Delta S^{\ddagger}_{off}$ appears lower for AT2 as compared to AT1 and NT. This means that the entropic component of the free energy for escape dictates the observed residence time difference between AT2 and the AT1/NT peptides while the enthalpy component could explain the difference in residence time for NT compared to AT1. One possible explanation for the entropic difference between angiotensin peptides is that the AT1 can exhibit a β-fold while AT2 does not (*70*, *73*). Differences between the NT and angiotensin free energy components are less obvious with the absence of gold clusters, which is somewhat unexpected given the structural differences of the NT peptide (see fig. S6 in the Supplementary Materials).

To further explore differences between the peptides, we consider the gold-occupied case. Gold clusters do not have as strong an effect on residence time for peptides (Fig. 6A) as they do for PEG (Fig. 4A).

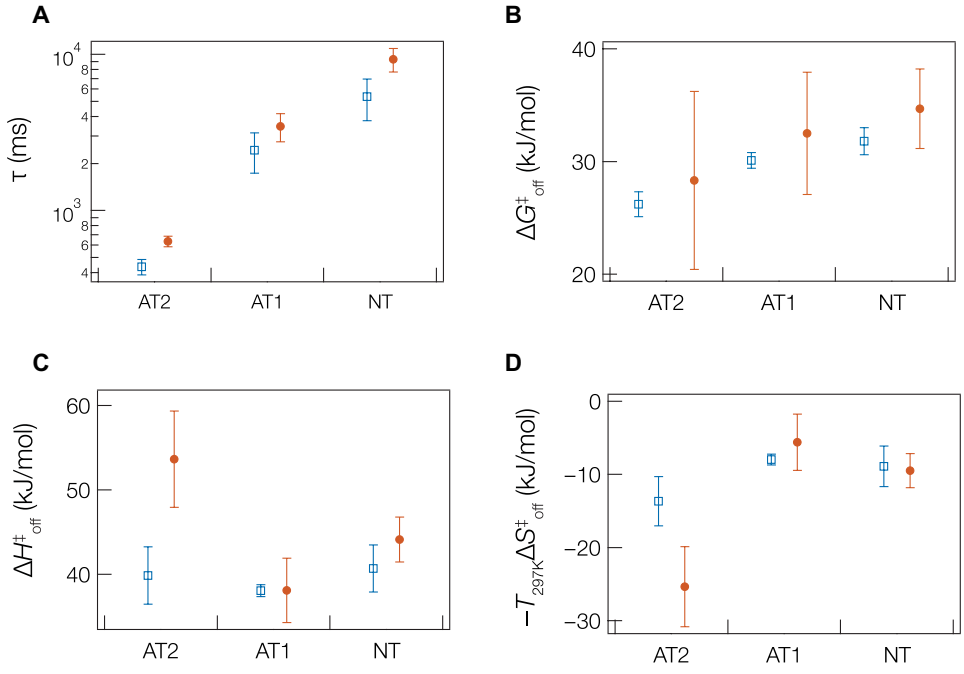

Fig. 6. Peptide mean residence times and corresponding enthalpy and entropy components of the free energy barrier to escape for the open (blue squares) and cluster-occupied (orange circles) pore. (**A**) Mean residence times for AT2, AT1, and NT show a residence time increasing with mass. Gold cluster inclusion increases the residence time moderately (two- to threefold) for all peptides. (**B**) Corresponding overall free energy of escape for the three peptides shows little effect from the gold cluster and a slight increase with increasing peptide size. (**C**) $\Delta H^{\ddagger}_{off}$ is unaffected by the gold cluster, but there is a clear dependence observed between different peptides. (**D**) $-T\Delta S^{\ddagger}_{off}$ mirrors the $\Delta H^{\ddagger}_{off}$ dependence with the entropy uniformly decreasing the free energy barrier. See the main text for details. All data were taken in 3 M KCl at pH 7.2 for AT1 and AT2 and pH 5.8 for NT, under a 70-mV applied transmembrane potential. Error bars show ±1 SE calculated from $n = 3$ different pores.

The ratio $\tau_{gold}/\tau_{open} \approx 3$ for peptides and $\tau_{gold}/\tau_{open} \approx 10$ for PEG. Despite the relatively small effect that the clusters have on the peptide residence times, there are differences in the free energy components that highlight the chemical and structural differences of these molecules. Figure 6 (C and D) shows that the gold cluster produces a substantial increase in the enthalpy that is opposed by a decrease in the entropy for the AT2. These effects are not observed for the larger peptides (AT1, NT) likely because AT2 is the only peptide tested that is small enough to interact with the cis-side gold cluster across the constriction under the moderate applied electric fields used here.

The results in Fig. 6 and fig. S5 highlight notable differences in the energy profiles of PEG and the peptides studied here. However, comparisons between peptides yield unusually similar free energy components with only subtle changes observed in the entropy and enthalpy. The angiotensin peptides show slight differences in entropy while NT shows a slight difference in enthalpy. The NMR structures for each peptide suggest that these differences may be driven by hydrogen bonding within each peptide; however, a more detailed chemical analysis will require additional tools (e.g., MD simulations) to extract a fuller picture of the peptide-pore interactions. Nevertheless, the free energy results here show a more nuanced understanding of the dynamics of the system and can serve as a step-off point to further develop greater specificity for designing nanopore-based peptide biosensors.

DISCUSSION

Polymer-pore interactions represent a ubiquitous phenomenon across several branches of physical and life sciences. The advent of nanopore sensing enables one to study these interactions at the single-molecule limit. Techniques for studying the free energy barrier to polymer escape from the pore have been limited, but here we describe a laser-based approach to localized heating that enables accurate and rapid control of the solution temperature. By using a dynamic heating approach, a fully realized statistical thermodynamic measurement can be performed even on inherently unstable systems, which is inaccessible for methods that rely on thermal control of bulk solution. When we applied this method to examine polymer systems, a detailed picture of the chemical interaction emerges (Fig. 7).

For the case of PEG, we have shown the critical role that entropy plays in the polymer-pore interaction. These results show that there is little hydrogen bonding between the polymer and the pore, rather the retention is primarily limited by the decreased entropy of the polymer as it exits the pore. This is highlighted by the observed changes with ionic strength, which modifies the solution conditions near the pore mouth in such a way as to reduce the entropic spring driving the polymer from the pore, provided that the PEG binds cations reversibly. In addition, we used this technique to measure the effect of reversible pore modifiers such as anionic gold clusters. Our results show that the enthalpic binding from Coulombic interactions plays a critical role in the enhancement and suggests that modifications to the local charge density within the pore present a path toward enhancing PEG sensing. Schemes involving electrostatic interactions have shown promise for nanopore sensing (*74*–*77*), and direct measurement of the thermodynamic properties should enable these interactions to be fine-tuned for the development of new pores.

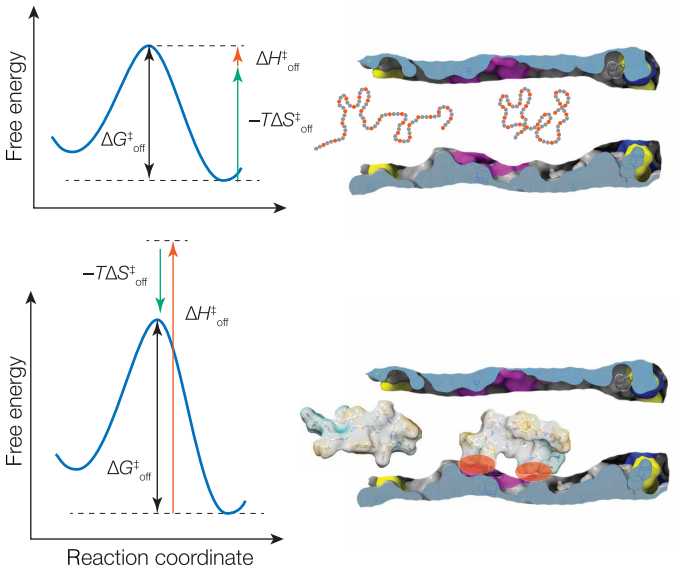

Fig. 7. The energetics of escape for PEG and peptides highlight the different chemistry of each molecule. (**Top**) PEG_{28} escape is an entropic process governed by the polymer interactions with the electrolyte. (**Bottom**) AT1, escape times are governed primarily by enthalpy, as highlighted by hypothetical hydrogen bonding between the polymer and the pore. A complete summary of the free energy profiles for all molecules and conditions studied herein is available in the Supplementary Materials.

Peptides were also studied, and it was shown that the free energy barrier for escape is dominated by enthalpy, which suggests hydrogen bonding between the peptides and the pore interior. These bonds lead to reduced entropy of the polymer in the pore, which is relaxed when the hydrogen bonds are broken during polymer escape. Thus, for the peptides, entropy favors escape while enthalpy favors retention. This is different from the noninteracting PEG, in which entropy dictates the barrier, with enthalpy providing a relatively small modification. It is worth noting that some component of the differences in the mean residence times between the different peptides may result from differences in the escape times τ_0 rather than differences in the energetics. Nevertheless, the thermodynamic studies here enable one to extract the free energy profile. Last, we studied the interaction of peptides with cluster-occupied pores and found that the interaction between the peptides and clusters was essentially nonexistent (with the exception of AT2 where the enthalpic gain was offset by the entropic loss) explaining the reduced enhancement in cluster-occupied residence times seen for the peptides as compared to PEG. In summary, the laser-based dynamic temperature probing described here effectively answers numerous questions about the nature of polymer-pore interactions and will lead to improved development of more efficient nanopore sensors and a better understanding of polymer-pore interactions.

MATERIALS AND METHODS

The experiment is performed on an inverted microscope (Zeiss Axio Observer D, Carl Zeiss, Germany) to enable clear optical access to the membrane support. The lipid bilayer membranes [DPhyPC (10 mg/ml; Avanti, Alabaster, AL) in hexadecane] are formed by a previously described painting method (*8*). The top and bottom chambers are filled with matching electrolyte solutions, and a Teflon sheet with a 50-μm hole (Eastern Scientific LLC, Rockville, MD) is positioned ≈200 μm above the bottom chamber coverslip. Following a previously described method for inserting single channels into membranes (*78*), a microforge (Warner Instruments, Hamden, CT) is used to create a small glass bead (ca. 150 μm) at the end of a micropipette. The bead is placed in a 500-nl drop of αHL (0.5 mg/ml; List Biological, Campbell, CA) solution for approximately 5 min. The droplet evaporates, resulting in adsorbed protein monomers on the glass bead. Using a motorized manipulator (MPC-325, Sutter Instruments, Novato, CA), the αHL-loaded glass bead is positioned over the membrane and lowered until it makes contact with the membrane. Ionic current is monitored for αHL pore formation. If multiple pores are inserted into the membrane, the protein-covered bead is removed and the membrane is reformed with a second lipid-covered glass bead. This process is repeated until a single stable pore is inserted into the membrane (typically fewer than five attempts). An *I-V* curve is recorded to verify the orientation of the αHL pore (cis-side up) (*79*).

Collimated light from a 200-mW continuous-wave, 1444-nm diode laser (MILIII-1444, Opto Engine, Midvale, UT) is aligned into an AOM (PN:1040AF-AIFO-1.0, Gooch & Housego, Ilminster, UK) where a sinusoidal wave (250 mHz) modulates the outgoing laser intensity. The light is launched through the back aperture of a 4× microscope objective (20% transmission at 1444 nm, Plan Achromat, Thorlabs, Newton, NJ) mounted onto the inverted microscope. All reported laser powers are measured with a meter (PN: S122c, Thorlabs) located at the entry port of the objective. The beam focus appears as a purple spot on a charge-coupled device camera (PN: DCU223C, Thorlabs), slightly larger than the 50-μm hole in the Teflon sheet, which provides approximately uniform heating across the entire lipid membrane. The temperature is measured from a calibration curve that connects the open pore current to the solution temperature. Details regarding this calibration can be found in the Supplementary Materials (*31*).

The gold clusters used here are $Au_{25}(SG)_{18}$ with a diameter on the order of 2.4 nm. The synthesis and characterization details have been previously described (*8*). For gold cluster insertion, the opening aperture of a micropipette tip containing ca. 30 μM concentration of $Au_{25}(SG)_{18}$ clusters is positioned ≈50 μm above the bilayer membrane. A small backing pressure (15 hPa) is applied to eject clusters toward the nanopore (Femtojet, Eppendorf, Enfield, CT). At this concentration, the pore is in the gold-occupied state approximately 50% of the time. A typical experiment lasts for ≈5 min, and unless stated otherwise, the lower chamber (trans-side) contains polymer analyte at various concentrations ([PEG_{28}] = 2.5 μM or [peptide] = 20 μM). Transmembrane voltages are applied across the lipid bilayer membrane with electrical ground fixed on the trans-side of the membrane. Details for the data analysis can be found in the Supplementary Materials.

SUPPLEMENTARY MATERIALS

Supplementary material for this article is available at http://advances.sciencemag.org/cgi/content/full/7/17/eabf5462/DC1

View/request a protocol for this paper from *Bio-protocol*.

REFERENCES AND NOTES

1. C. K. Colton, C. N. Satterfield, C.-J. Lai, Diffusion and partitioning of macromolecules within finely porous glass. *AIChE J.* **21**, 289–298 (1975).

2. M. Daoud, P. G. de Gennes, Statistics of macromolecular solutions trapped in small pores. *J. Phys.* **38**, 85–93 (1977).
3. F. Brochard, P. G. DeGennes, Dynamics of confined polymer-chains. *J. Chem. Phys.* **67**, 52–56 (1977).
4. S. M. Bezrukov, I. Vodyanoy, V. A. Parsegian, Counting polymers moving through a single-ion channel. *Nature* **370**, 279–281 (1994).
5. S. Bezrukov, J. J. Kasianowicz, Current noise reveals protonation kinetics and number of ionizable sites in an open protein ion channel. *Phys. Rev. Lett.* **70**, 2352–2355 (1993).
6. S. M. Bezrukov, I. Vodyanoy, R. Brutyan, J. J. Kasianowicz, Dynamics and free energy of polymers partitioning into a nanoscale pore. *Macromolecules* **29**, 8517–8522 (1996).
7. J. J. Kasianowicz, J. W. F. Robertson, E. R. Chan, J. E. Reiner, V. M. Stanford, Nanoscopic porous sensors. *Annu. Rev. Anal. Chem.* **1**, 737–766 (2008).
8. C. E. Angevine, A. E. Chavis, N. Kothalawala, A. Dass, J. E. Reiner, Enhanced single molecule mass spectrometry via charged metallic clusters. *Anal. Chem.* **86**, 11077–11085 (2014).
9. H. Mökkönen, T. Ikonen, T. Ala-Nissila, H. Jónsson, Transition state theory approach to polymer escape from a one dimensional potential well. *J. Chem. Phys.* **142**, 224906 (2015).
10. D. P. Hoogerheide, P. A. Gurnev, T. K. Rostovtseva, S. M. Bezrukov, Mechanism of α-synuclein translocation through a VDAC nanopore revealed by energy landscape modeling of escape time distributions. *Nanoscale* **9**, 183–192 (2017).
11. N. J. Yang, M. J. Hinner, Getting across the cell membrane: An overview for small molecules, peptides, and proteins. *Methods Mol. Biol.* **1266**, 29–53 (2015).
12. D. K. Lubensky, D. R. Nelson, Driven polymer translocation through a narrow pore. *Biophys. J.* **77**, 1824–1838 (1999).
13. O. Dudko, A. Filippov, J. Klafter, M. Urbakh, Dynamic force spectroscopy: A Fokker-Planck approach. *Chem. Phys. Lett.* **352**, 499–504 (2002).
14. J. M. Polson, T. R. Dunn, Evaluating the applicability of the Fokker-Planck equation in polymer translocation: A Brownian dynamics study. *J. Chem. Phys.* **140**, 184904 (2014).
15. M. Muthukumar, Polymer escape through a nanopore. *J. Chem. Phys.* **118**, 5174–5184 (2003).
16. M. Muthukumar, C. Y. Kong, Simulation of polymer translocation through protein channels. *Proc. Natl. Acad. Sci. U.S.A.* **103**, 5273–5278 (2006).
17. M. Muthukumar, Polymer translocation through a hole. *J. Chem. Phys.* **111**, 10371–10374 (1999).
18. E. Slonkina, A. B. Kolomeisky, Polymer translocation through a long nanopore. *J. Chem. Phys.* **118**, 7112–7118 (2003).
19. S. Matysiak, A. Montesi, M. Pasquali, A. B. Kolomeisky, C. Clementi, Dynamics of polymer translocation through nanopores: Theory meets experiment. *Phys. Rev. Lett.* **96**, 118103 (2006).
20. J. E. Reiner, J. J. Kasianowicz, B. J. Nablo, J. W. F. Robertson, Theory for polymer analysis using nanopore-based single-molecule mass spectrometry. *Proc. Natl. Acad. Sci. U.S.A.* **107**, 12080–12085 (2010).
21. A. M. Berezhkovskii, S. M. Bezrukov, On the applicability of entropy potentials in transport problems. *Eur. Phys. J. Spec. Top.* **223**, 3063–3077 (2014).
22. P. Jun Park, W. Sung, Dynamics of a polymer surmounting a potential barrier: The Kramers problem for polymers. *J. Chem. Phys.* **111**, 5259–5266 (1999).
23. G. Maglia, M. R. Restrepo, E. Mikhailova, H. Bayley, Enhanced translocation of single DNA molecules through α-hemolysin nanopores by manipulation of internal charge. *Proc. Natl. Acad. Sci. U.S.A.* **105**, 19720–19725 (2008).
24. M. Ali, B. Schiedt, K. Healy, R. Neumann, W. Ensinger, Modifying the surface charge of single track-etched conical nanopores in polyimide. *Nanotechnology* **19**, 085713 (2008).
25. M. F. Breton, F. Discala, L. Bacri, D. Foster, J. Pelta, A. Oukhaled, Exploration of neutral versus polyelectrolyte behavior of poly(ethylene glycol)s in alkali ion solutions using single-nanopore recording. *J. Phys. Chem. Lett.* **4**, 2202–2208 (2013).
26. D. W. Deamer, D. Branton, Characterization of nucleic acids by nanopore analysis. *Acc. Chem. Res.* **35**, 817–825 (2002).
27. Y. Jung, H. Bayley, L. Movileanu, Temperature-responsive protein pores. *J. Am. Chem. Soc.* **128**, 15332–15340 (2006).
28. D. K. Lathrop, E. N. Ervin, G. A. Barrall, M. G. Keehan, R. Kawano, M. A. Krupka, H. S. White, A. H. Hibbs, Monitoring the escape of DNA from a nanopore using an alternating current signal. *J. Am. Chem. Soc.* **132**, 1878–1885 (2010).
29. L. Payet, M. Martinho, C. Merstorf, M. Pastoriza-Gallego, J. Pelta, V. Viasnoff, L. Auvray, M. Muthukumar, J. Mathe, Temperature effect on ionic current and ssDNA transport through nanopores. *Biophys. J.* **109**, 1600–1607 (2015).
30. F. Piguet, H. Ouldali, F. Discala, M.-F. Breton, J. C. Behrends, J. Pelta, A. Oukhaled, High temperature extends the range of size discrimination of nonionic polymers by a biological nanopore. *Sci. Rep.* **6**, 38675 (2016).
31. C. E. Angevine, S. J. Seashols-Williams, J. E. Reiner, Infrared laser heating applied to nanopore sensing for DNA duplex analysis. *Anal. Chem.* **88**, 2645–2651 (2016).
32. J. Yao, B. Liu, F. Qin, Rapid temperature jump by infrared diode laser irradiation for patch-clamp studies. *Biophys. J.* **96**, 3611–3619 (2009).
33. J. E. Reiner, J. W. F. Robertson, D. L. Burden, L. K. Burden, A. Balijepalli, J. J. Kasianowicz, Temperature sculpting in yoctoliter volumes. *J. Am. Chem. Soc.* **135**, 3087–3094 (2013).
34. C. R. Crick, P. Albella, B. Ng, A. P. Ivanov, T. Roschuk, M. P. Cecchini, F. Bresme, S. A. Maier, J. B. Edel, Precise attoliter temperature control of nanopore sensors using a nanoplasmonic bullseye. *Nano Lett.* **15**, 553–559 (2015).
35. H. Yamazaki, R. Hu, R. Y. Henley, J. Halman, K. A. Afonin, D. Yu, Q. Zhao, M. Wanunu, Label-free single-molecule thermoscopy using a laser-heated nanopore. *Nano Lett.* **17**, 7067–7074 (2017).
36. L. Movileanu, S. Cheley, H. Bayley, Partitioning of individual flexible polymers into a nanoscopic protein pore. *Biophys. J.* **85**, 897–910 (2003).
37. M. G. Larimi, L. A. Mayse, L. Movileanu, Interactions of a polypeptide with a protein nanopore under crowding conditions. *ACS Nano* **13**, 4469–4477 (2019).
38. H. Berg, E. M. Purcell, Physics of chemoreception. *Biophys. J.* **20**, 193–219 (1977).
39. M. Muthukumar, Theory of capture rate in polymer translocation. *J. Chem. Phys.* **132**, 195101 (2010).
40. A. Balijepalli, J. W. F. Robertson, J. E. Reiner, J. J. Kasianowicz, R. W. Pastor, Theory of polymer-nanopore interactions refined using molecular dynamics simulations. *J. Am. Chem. Soc.* **135**, 7064–7072 (2013).
41. D. G. Truhlar, B. C. Garrett, S. J. Klippenstein, Current status of transition-state theory. *J. Phys. Chem.* **100**, 12771–12800 (1996).
42. A. E. Chavis, K. T. Brady, G. A. Hatmaker, C. E. Angevine, N. Kothalawala, A. Dass, J. W. F. Robertson, J. E. Reiner, Single molecule nanopore spectrometry for peptide detection. *ACS Sens.* **2**, 1319–1328 (2017).
43. L. Song, M. R. Hobaugh, C. Shustak, S. Cheley, H. Bayley, J. E. Gouaux, Structure of staphylococcal α-hemolysin, a heptameric transmembrane pore. *Science* **274**, 1859–1865 (1996).
44. S. Y. Noskov, W. Im, B. Roux, Ion permeation through the alpha-hemolysin channel: Theoretical studies based on Brownian dynamics and Poisson-Nernst-Plank electrodiffusion theory. *Biophys. J.* **87**, 2299–2309 (2004).
45. S. M. Bezrukov, O. V. Krasilnikov, L. N. Yuldasheva, A. M. Berezhkovskii, C. G. Rodrigues, Field-dependent effect of crown ether (18-Crown-6) on ionic conductance of α-hemolysin channels. *Biophys. J.* **87**, 3162–3171 (2004).
46. O. V. Krasilnikov, C. G. Rodrigues, S. M. Bezrukov, Single polymer molecules in a protein nanopore in the limit of a strong polymer-pore attraction. *Phys. Rev. Lett.* **97**, 018301 (2006).
47. J. W. F. Robertson, C. G. Rodrigues, V. M. Stanford, K. A. Rubinson, O. V. Krasilnikov, J. J. Kasianowicz, Single-molecule mass spectrometry in solution using a solitary nanopore. *Proc. Natl. Acad. Sci. U.S.A.* **104**, 8207–8211 (2007).
48. J. W. F. Robertson, J. J. Kasianowicz, J. E. Reiner, Changes in ion channel geometry resolved to sub-Ångström precision via single molecule mass spectrometry. *J. Phys. Condens. Matter.* **22**, 454108 (2010).
49. A. M. Berezhkovskii, M. A. Pustovoit, S. M. Bezrukov, Entropic effects in channel-facilitated transport: Interparticle interactions break the flux symmetry. *Phys. Rev. E.* **80**, 020904 (2009).
50. Z. E. Dell, M. Muthukumar, Macromolecule translocation in a nanopore: Center of mass drift–diffusion over an entropic barrier. *bioRxiv* 10.1101/667816 , (2019).
51. X. Liu, M. Mihovilovic Skanata, D. Stein, Entropic cages for trapping DNA near a nanopore. *Nat. Commun.* **6**, 6222 (2015).
52. M. H. Lam, K. Briggs, K. Kastritis, M. Magill, G. R. Madejski, J. L. McGrath, H. W. de Haan, V. Tabard-Cossa, Entropic trapping of DNA with a nanofiltered nanopore. *ACS Appl. Nano Mater.* **2**, 4773–4781 (2019).
53. C. G. Rodrigues, D. C. Machado, S. F. Chevtchenko, O. V. Krasilnikov, Mechanism of KCl enhancement in detection of nonionic polymers by nanopore sensors. *Biophys. J.* **95**, 5186–5192 (2008).
54. A. Aksimentiev, K. Schulten, Imaging alpha-hemolysin with molecular dynamics: Ionic conductance, osmotic permeability, and the electrostatic potential map. *Biophys. J.* **88**, 3745–3761 (2005).
55. P.-G. DeGennes, *Scaling Concepts in Polymer Physics* (Cornell Univ. Press, 1979).
56. J. E. Mark, P. Flory, Configuration of polyoxyethylene chain. *J. Am. Chem. Soc.* **87**, 1415–1423 (1965).
57. H. Lee, R. M. Venable, A. D. MacKerell Jr., R. W. Pastor, Molecular dynamics studies of polyethylene oxide and polyethylene glycol: Hydrodynamic radius and shape anisotropy. *Biophys. J.* **95**, 1590–1599 (2008).
58. J. H. Forstater, K. Briggs, J. W. F. Robertson, J. Ettedgui, O. Marie-Rose, C. Vaz, J. J. Kasianowicz, V. Tabard-Cossa, A. Balijepalli, MOSAIC: A modular single-molecule analysis interface for decoding multistate nanopore data. *Anal. Chem.* **88**, 11900–11907 (2016).
59. K. Devanand, J. C. Selser, Asymptotic behavior and long-range interactions in aqueous solutions of poly(ethylene oxide). *Macromolecules* **24**, 5943–5947 (1991).
60. J. W. F. Robertson, J. E. Reiner, The utility of nanopore technology for protein and peptide sensing. *Proteomics* **18**, 1800026 (2018).

61. K. Willems, V. Van Meervelt, C. Wloka, G. Maglia, Single-molecule nanopore enzymology. *Philos. Trans. R. Soc. Lond. B Biol. Sci.* **372**, 20160230 (2017).
62. G. Huang, K. Willems, M. Soskine, C. Wloka, G. Maglia, Electro-osmotic capture and ionic discrimination of peptide and protein biomarkers with FraC nanopores. *Nat. Commun.* **2017**, 935 (2017).
63. M. Soskine, A. Biesemans, G. Maglia, Single-molecule analyte recognition with ClyA nanopores equipped with internal protein adaptors. *J. Am. Chem. Soc.* **137**, 5793–5797 (2015).
64. C. Cao, J. Yu, Y.-Q. Wang, Y.-L. Ying, Y.-T. Long, Driven translocation of polynucleotides through an aerolysin nanopore. *Anal. Chem.* **88**, 5046–5049 (2016).
65. E. C. Yusko, J. M. Johnson, S. Majd, P. Prangkio, R. C. Rollings, J. Li, J. Yang, M. Mayer, Controlling protein translocation through nanopores with bio-inspired fluid walls. *Nat. Nanotechnol.* **6**, 253–260 (2011).
66. E. C. Yusko, B. R. Bruhn, O. M. Eggenberger, J. Houghtaling, R. C. Rollings, N. C. Walsh, S. Nandivada, M. Pindrus, A. R. Hall, D. Sept, J. Li, D. S. Kalonia, M. Mayer, Real-time shape approximation and fingerprinting of single proteins using a nanopore. *Nat. Nanotechnol.* **12**, 360–367 (2017).
67. H. Ouldali, K. Sarthak, T. Ensslen, F. Piguet, P. Manivet, J. Pelta, J. C. Behrends, A. Aksimentiev, A. Oukhaled, Electrical recognition of the twenty proteinogenic amino acids using an aerolysin nanopore. *Nat. Biotechnol.* **38**, 176–181 (2020).
68. S. Li, C. Cao, J. Yang, Y.-T. Long, Detection of peptides with different charges and lengths by using the aerolysin nanopore. *ChemElectroChem* **6**, 126–129 (2019).
69. J. Coutant, P. A. Curmi, F. Toma, J.-P. Monti, NMR solution structure of neurotensin in membrane-mimetic environments: Molecular basis for neurotensin receptor recognition. *Biochemistry* **46**, 5656–5663 (2007).
70. G. A. Spyroulias, P. Nikolakopoulou, A. Tzakos, I. P. Gerothanassis, V. Magafa, E. Manessi-Zoupa, P. Cordopatis, Comparison of the solution structures of angiotensin I & II. *Eur. J. Biochem.* **270**, 2163–2173 (2003).
71. S. K. Lakkaraju, W. Hwang, Critical buckling length versus persistence length: What governs biofilament conformation? *Phys. Rev. Lett.* **102**, 118102 (2009).
72. B. Schuler, E. A. Lipman, P. J. Steinbach, M. Kumke, W. A. Eaton, Polyproline and the "spectroscopic ruler" revisited with single-molecule fluorescence. *Proc. Natl. Acad. Sci. U.S.A.* **102**, 2754–2759 (2005).
73. L. Mereuta, A. Asandei, C. H. Seo, Y. Park, T. Luchian, Quantitative understanding of pH- and salt-mediated conformational folding of histidine-containing, β-hairpin-like peptides, through single-molecule probing with protein nanopores. *ACS Appl. Mater. Interfaces* **6**, 13242–13256 (2014).
74. M. M. Mohammad, S. Prakash, A. Matouschek, L. Movileanu, Controlling a single protein in a nanopore through electrostatic traps. *J. Am. Chem. Soc.* **130**, 4081–4088 (2008).
75. L. Harrington, S. Cheley, L. T. Alexander, S. Knapp, H. Bayley, Stochastic detection of Pim protein kinases reveals electrostatically enhanced association of a peptide substrate. *Proc. Natl. Acad. Sci. U.S.A.* **110**, E4417–E4426 (2013).
76. M. A. Fahie, M. Chen, Electrostatic interactions between OmpG nanopore and analyte protein surface can distinguish between glycosylated isoforms. *J. Phys. Chem. B* **119**, 10198–10206 (2015).
77. S. F. Buchsbaum, N. Mitchell, H. Martin, M. Wiggin, A. Marziali, P. V. Coveney, Z. Siwy, S. Howorka, Disentangling steric and electrostatic factors in nanoscale transport through confined space. *Nano Lett.* **13**, 3890–3896 (2013).
78. M. A. Holden, H. Bayley, Direct introduction of single protein channels and pores into lipid bilayers. *J. Am. Chem. Soc.* **127**, 6502–6503 (2005).
79. S. Bhattacharya, J. Muzard, L. Payet, J. Mathé, U. Bockelmann, A. Aksimentiev, V. Viasnoff, Rectification of the current in α-hemolysin pore depends on the cation type: The alkali series probed by molecular dynamics simulations and experiments. *J. Phys. Chem. C* **115**, 4255–4264 (2011).
80. R. J. White, E. N. Ervin, T. Yang, X. Chen, S. Daniel, P. S. Cremer, H. S. White, Single ion-channel recordings using glass nanopore membranes. *J. Am. Chem. Soc.* **129**, 11766–11775 (2007).
81. O. V. Krasilnikov, R. Z. Sabirov, V. I. Ternovsky, P. G. Merzliak, B. A. Tashmukhamedov, The structure of *Staphylococcus aureus* alpha-toxin-induced ionic channel. *Gen. Physiol. Biophys.* **7**, 467–473 (1988).
82. A. Balijepalli, J. Ettedgui, A. T. Cornio, J. W. F. Robertson, K. P. Cheung, J. J. Kasianowicz, C. Vaz, Quantifying short-lived events in multistate ionic current measurements. *ACS Nano* **8**, 1547–1553 (2014).
83. O. Hosoya, S. Chono, Y. Saso, K. Juni, K. Morimoto, T. Seki, Determination of diffusion coefficients of peptides and prediction of permeability through a porous membrane. *J. Pharm. Pharmacol.* **56**, 1501–1507 (2004).
84. K. Shimada, H. Kato, T. Saito, S. Matsuyama, S. Kinugasa, Precise measurement of the self-diffusion coefficient for poly(ethylene glycol) in aqueous solution using uniform oligomers. *J. Chem. Phys.* **122**, 244914 (2005).
85. T. D. Goddard, C. C. Huang, E. C. Meng, E. F. Pettersen, G. S. Couch, J. H. Morris, T. E. Ferrin, UCSF ChimeraX: Meeting modern challenges in visualization and analysis. *Protein Sci.* **27**, 14–25 (2018).

Acknowledgments: We thank M. Zwolak and D. Hoogerheide for helpful discussions and N. Kothalawala for synthesis and characterization of the $Au_{25}(SG)_{18}$ clusters. **Funding:** This material is based on work supported by the National Science Foundation under grants CBET-2011173 and NSF-1808138. **Author contributions:** C.E.A. and J.E.R. designed research; C.E.A., J.W.F.R., A.D., and J.E.R. performed research; A.D. contributed new reagents; C.E.A., J.W.F.R., and J.E.R. analyzed data; C.E.A., J.W.F.R., and J.E.R. wrote the paper. **Competing interests:** The authors declare that they have no competing interests. **Data and materials availability:** All data needed to evaluate the conclusions in the paper are present in the paper and/or the Supplementary Materials. Additional data related to this paper may be requested from the authors.

Submitted 3 November 2020
Accepted 4 March 2021
Published 21 April 2021
10.1126/sciadv.abf5462

Citation: C. E. Angevine, J. W. F. Robertson, A. Dass, J. E. Reiner, Laser-based temperature control to study the roles of entropy and enthalpy in polymer-nanopore interactions. *Sci. Adv.* **7**, eabf5462 (2021).